Joint Waveform/Receiver Design for Vital-Sign Detection in Signal-Dependent Interference

Gabriel Beltrão
SnT
University of Luxembourg
Luxembourg
gabriel.tedgue-beltrao@uni.lu

Mohammad Alaee-Kerahroodi
SnT
University of Luxembourg
Luxembourg
mohammad.alaee@uni.lu

Udo Schroeder
IEE S.A.
Luxembourg
udo.schroeder@iee.lu

Bhavani Shankar M.R.
SnT
University of Luxembourg
Luxembourg
bhavani.shankar@uni.lu

***Abstract*—This paper presents the joint design of discrete slow-time radar waveform and receive filter, with the aim of enhancing the Signal to Interference and Noise Ratio (SINR) in phase coded radar systems for vital-sign monitoring. Towards this, we consider maximizing the SINR at the input of the vital-sign estimation block, when transmitting hardware efficient M-ary Phase Shift Keying (MPSK) sequences. This multi-variable and non-convex optimization problem is efficiently solved based on a Minimum Variance Distortionless Response (MVDR) filter, with the Coordinate Descent (CD) approach for the sequence optimization, and the obtained results have shown attractive interference suppression capabilities, even for the simple binary case.**

I. Introduction

The non-contact monitoring of the cardiorespiratory activity provides several advantages over standard devices. It neither confines nor inhibits the subject, and does not cause any discomfort, skin damage or irritation as electrodes, adhesive sensors or straps could do [1]. This is especially important in the case of neonates and people with sensitive skin, as well as for long-term monitoring. Additionally, the reliability can also be increased since patients are unaware of the measurements and, therefore, less likely to, intentionally or not, alter their breathing and heartbeat rates [2]. In this context, several applications using Doppler radars have been recently proposed. Besides monitoring newborns and infants [3], this type of system can also be applied for driver monitoring [4]–[6], occupancy detection [7] and human location [8].

The activity of the cardiovascular and respiratory systems causes some physical and physiological effects on the human body [9]. The volumetric changes of the heart muscle when pumping blood through the circulatory system can be transmitted to the chest leading to a subtle movement. The chest also moves during the inspiration/expiration cycle, as a result of the diaphragm muscle movement. These small and periodic movements can be detected by the radar, allowing accurate estimation of the breathing and heartbeat rates in certain conditions. However, due to the reduced amplitudes, the receiving signal can be easily buried in the background noise [10], or masked by strong interference arising from the external environment, or even from the body itself [11].

In this context, many techniques have been proposed for improving vital-signs detection and estimation [12]–[15]. However, most of them are focused exclusively on signal processing techniques on the receiver side and, despite promising results, there are still some open questions. Joint waveform and receiver design is one of the key techniques that allows to fully explore the capabilities of future radar systems [16]–[18], and, until now, it has not yet been formally addressed for vital-sign monitoring.

Based on the previous work from [19], this paper attempts to fill this relevant gap by proposing a slow-time joint waveform and receiver filter design for maximizing the Signal to Interference and Noise Ratio (SINR) for breathing or heartbeat estimation, in the presence of signal dependent interference. Additionally, further motivated by many recent work [20], [21], we are imposing the use of a discrete M-ary Phase Shift Keying (MPSK) alphabet, which is an attractive constraint from a practical point-of-view.

The remainder of this paper is organized as follows. In section II, we introduce the system model and problem formulation. Section III presents the proposed joint design of waveform and receive filter, and its performance is numerically assessed in section IV. Finally, in Section V, some conclusions are drawn.

A. Notation

We are adopting the following notation: boldface for vectors $\boldsymbol{x}$ (lower case), and for matrices $\boldsymbol{X}$ (upper case). $\odot$ denotes the Hadamard product. The transpose, the conjugate, and the conjugate transpose operators are denoted by the symbols $(.)^T$, $(.)^*$, and $(.)^H$, respectively, while $\mathbb{C}^N$ and $\mathbb{R}^N$ are the sets of N-dimensional vectors of complex and real numbers. The $diag(\boldsymbol{x})$ indicates the diagonal matrix of $\boldsymbol{x}$, and $\boldsymbol{I}$ denotes the identity matrix with size determined from the context. The Euclidean norm of the vector $\boldsymbol{x}$ is denoted by $||\boldsymbol{x}||$. The letter j represents the imaginary unit (i.e., $j = \sqrt{-1}$). $\mathbb{E}[.]$ denotes the statistical expectation. Finally, for any optimization problem $\mathcal{P}$, $v(\mathcal{P})$ represents its optimal value.

978-1-7281-8942-0/20/$31.00

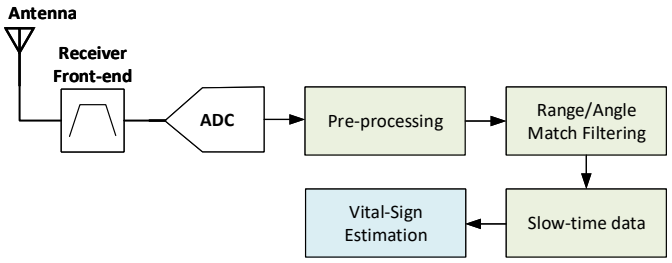

Fig. 1: Standard phase-coded pulse-based radar block diagram.

II. System Model

Radar-based remote monitoring of vital signs usually relies on the phase analysis of the received signal from a given target of interest. In the specific case of breathing and heartbeat monitoring, the transmitted waveform is phase-modulated by the chest-wall displacement caused by the periodic movement of the diaphragm and the heart. Figure 1 shows the standard block diagram for the receiver of a phase coded pulse-based radar system. Following the transmission of N pulses during a Coherent Processing Interval (CPI), the received waveform is down-converted to baseband and sampled at the receiver front end. The resultant I/Q samples usually undergo some pre-processing operations before the range/angle matched filtering and detection.

The received baseband signal corresponding to the m^{th} transmitted pulse can be written as [22]

$$y_m(t) = ka_m[t - mT_I - \frac{2R(t)}{c}]e^{j[\phi_m(t) - \frac{4\pi}{\lambda}R(t)]} \tag{1}$$

where k is a complex parameter accounting for the channel propagation and backscattering effects from the target, $a_m(t)$ and $\phi_m(t)$ are respectively the amplitude and phase of the transmitted fast-time pulse, T_I is the Pulse Repetition Interval (PRI) and $R(t)$ denotes the target range. Additionally, c is the speed of light and λ the operating wavelength. After range matched filtering, assuming no range migration during the CPI, and further assuming no appreciable phase change during fast-time [23], the m^{th} sample in the target range-azimuth cell can be expressed as

$$y(m) = \hat{k}e^{-j\frac{4\pi}{\lambda}R_0}s(m)e^{-j\frac{4\pi}{\lambda}x(mT_I)} \tag{2}$$

where the constant $\hat{k}$ combines k and the amplitude of the matched filter output, $s(m)$ is the m^{th} slow-time transmitted complex sample (with phase ϕ_m), R_0 is the target nominal range and $x(mT_I)$ represents the chest-wall displacement over time. Therefore, the N-dimensional slow-time column vector, containing the target information from the range-azimuth cell under test, can be written as [19]

$$\boldsymbol{y} = \alpha_r \boldsymbol{s} \odot \boldsymbol{p}_x + \boldsymbol{i}(\boldsymbol{s}) + \boldsymbol{n}, \tag{3}$$

where α_r now accounts for $\hat{k}$, and also for the constant phase term in (2), $\boldsymbol{s} = [s(1), s(2), ..., s(N)]^T \in \mathbb{C}^N$ is the transmitted radar code over the slow-time dimension and

$$\boldsymbol{p}_x = [1, e^{-j\frac{4\pi}{\lambda}x(T_I)}, ..., e^{-j\frac{4\pi}{\lambda}x[(N-1)T_I]}]^T \in \mathbb{C}^N \tag{4}$$

is the target spatial Doppler vector, containing the desired breathing or heartbeat signal. According to previous work [24]–[26], the displacement signal is usually assumed to be sinusoidal with constant amplitude and frequency for the duration of one CPI. Standard amplitude values are in the range of 4 mm to 12 mm for breathing [27] and 0.2 mm to 0.5 mm for heartbeat [28]. Breathing rates of healthy adults can vary from 5 to 20 breaths per minute (0.08-0.5 Hz), while the heartbeat can range from 60 to 120 beats per minute (1-2 Hz) [28].

While the noise vector $\boldsymbol{n}$ is being modeled as a zero-mean white Gaussian process, with autocorrelation matrix $\mathbb{E}\left[\boldsymbol{n}\boldsymbol{n}^H\right] = \sigma_n^2 I$, the vector $\boldsymbol{i}(\boldsymbol{s})$ contains the superposition of the returns from different scatterers, each from the $(r,k)^{th}$ range-azimuth bin, representing different subjects or moving objects in the same space, or even random movements from the body itself. It can be written as [29]

$$\boldsymbol{i}(\boldsymbol{s}) = \sum_{r=0}^{Nc-1}\sum_{k=0}^{L-1} \alpha_{(r,k)} \boldsymbol{J}_r(\boldsymbol{s} \odot \boldsymbol{p}_i), \tag{5}$$

where $N_c \leq N$ is the number of range rings that interfere with the range-azimuth bin of interest $(0,0)$, L is the number of discrete azimuth sectors, $\alpha_{(r,k)}$ and $\boldsymbol{p}_i = [1, e^{j2\pi\nu_{i_{(r,k)}}}, ..., e^{j2\pi(N-1)\nu_{i_{(r,k)}}}]^T \in \mathbb{C}^N$ are respectively the scatter complex amplitude and spatial Doppler vector in the range-azimuth bin (r,k), with $\nu_{i_{(r,k)}}$ its normalized Doppler frequency. Additionally, $\forall r \in \{0, ...N-1\}$, $\boldsymbol{J}_r$ is a Toeplitz matrix with the r^{th} diagonal being 1 and 0 elsewhere [30], responsible for time-shifting the interference signal according to the specific range position.

A. Problem Formulation

If the complex-signal demodulation [31] is used, the slow-time vector $\boldsymbol{y}$ can be used as the direct input to the vital-sign estimation block. Assuming that $\boldsymbol{y}$ is filtered with $\boldsymbol{w}$, the SINR at the output of the filter can be written as

$$\text{SINR} \equiv g(\boldsymbol{s}, \boldsymbol{w}) = \frac{|\alpha_r|^2 |\boldsymbol{w}^H(\boldsymbol{s} \odot \boldsymbol{p}_x)|^2}{\boldsymbol{w}^H \Sigma_{\boldsymbol{i}}(\boldsymbol{s}) \boldsymbol{w} + \sigma_n^2 ||\boldsymbol{w}||^2}, \tag{6}$$

where $\Sigma_{\boldsymbol{i}}(\boldsymbol{s})$ accounts for the signal-dependent interference covariance matrix. If the scatterers are uncorrelated, with $\mathbb{E}[\alpha_{(r,k)}] = 0$, and normalized Doppler frequency uniformly distributed around a mean value $\overline{\nu}_i$, with some uncertainty $\epsilon/2$, i.e. $\nu_i \sim \mathcal{U}(\overline{\nu}_i - \epsilon/2, \overline{\nu}_i + \epsilon/2)$, $\Sigma_{\boldsymbol{i}}(\boldsymbol{s})$ can be calculated as [29]

$$\boldsymbol{\Sigma}_{\boldsymbol{i}}(\boldsymbol{s}) = \mathbb{E}[\boldsymbol{i}\boldsymbol{i}^H] = \sum_{r=0}^{Nc-1}\sum_{k=0}^{L-1} \sigma_{(r,k)}^2 \boldsymbol{J}_r \boldsymbol{\Gamma}(\boldsymbol{s}, (r,k)) \boldsymbol{J}_r^H, \tag{7}$$

with $\sigma_{(r,k)}^2 = \mathbb{E}[|\alpha_{(r,k)}|^2]$ the mean interfering power at the $(r,k)^{th}$ range-azimuth cell, and

$$\boldsymbol{\Gamma}(\boldsymbol{s}, (r,k)) = diag\{\boldsymbol{s}\} \boldsymbol{\Phi}_{\epsilon_{(r,k)}}^{\overline{\nu}_{i_{(r,k)}}} diag\{\boldsymbol{s}\}^H, \tag{8}$$

where $\mathbf{\Phi}_{\epsilon_{(r,k)}}^{\overline{\nu}_{i_{(r,k)}}}$ is the covariance matrix of $\boldsymbol{p}_i(\nu_{i_{(r,k)}})$, given by

$$\mathbf{\Phi}_{\epsilon}^{\overline{\nu}_i}(l,m) = \begin{cases} 1, & \text{if } l = m \\ e^{(j2\pi\overline{\nu}_i(l-m))}\dfrac{[\sin\pi\epsilon(l-m)]}{[\pi\epsilon(l-m)]}, & \text{if } l \neq m \end{cases} \tag{9}$$

with $(l,m) \in \{1,...,N\}^2$. We propose the joint design of the slow-time radar code and the receive filter, with the aim of maximizing the SINR (in the presence of undesired interference), under the practical constraint of using discrete phase sequences from an MPSK alphabet. Our design can thus be formulated as the following constrained optimization problem

$$\mathcal{P}_1 \begin{cases} \max\limits_{\boldsymbol{s},\boldsymbol{w}} & g(\boldsymbol{s},\boldsymbol{w}), \\ s.t. & \boldsymbol{s} \in \Omega_M \end{cases} \tag{10}$$

where $\Omega_M = \{\boldsymbol{s} | s_i \in \Psi_M, i = 1,...,N\}$ represents the feasible set, i.e. the alphabet, and $\Psi_M = \{1, e^{j\frac{2\pi}{M}}, e^{j\frac{4\pi}{M}}, ..., e^{j\frac{2(M-1)\pi}{M}}\}$ defines MPSK sequences, with M being the alphabet size.

III. Joint Waveform and Receiver Design

In this section, we deal with the joint design of the radar code and the corresponding receive filter under a practical constraint on the phase of the transmit code sequences. Notice this is a multi-variable non-convex constrained optimization, and the technique we adopt is based on a sequential optimization procedure, iteratively optimizing the SINR [32]. Specifically, starting from an admissible radar code $\boldsymbol{s}^{(0)}$, we design the receive filter $\boldsymbol{w}^{(0)}$ which maximizes the SINR corresponding to the transmitted sequence $\boldsymbol{s}^{(0)}$. Once $\boldsymbol{w}^{(0)}$ is found, we search in the alphabet for an alternative sequence $\boldsymbol{s}^{(1)}$, and subsequently recalculate $\boldsymbol{w}^{(1)}$ for increasing the SINR and so on.

The problem $\mathcal{P}_{\boldsymbol{w}}^{(n)}$ of finding the receive filter $\boldsymbol{w}^{(n)}$ for an specific code $\boldsymbol{s}^{(n)}$ can thus be written as

$$\mathcal{P}_{\boldsymbol{w}}^{(n)} \begin{cases} \max\limits_{\boldsymbol{w}} & \dfrac{|\alpha_r|^2 |\boldsymbol{w}^H(\boldsymbol{s}^{(n)} \odot \boldsymbol{p}_x)|^2}{\boldsymbol{w}^H \Sigma_{\boldsymbol{i}}(\boldsymbol{s}^{(n)})\boldsymbol{w} + \sigma_n^2 ||\boldsymbol{w}||^2}. \end{cases} \tag{11}$$

In the same way, the problem $\mathcal{P}_{\boldsymbol{s}}^{(n)}$ of finding the best sequence $\boldsymbol{s}^{(n)}$ for an specific receive filter $\boldsymbol{w}^{(n)}$ can thus be written as

$$\mathcal{P}_{\boldsymbol{s}}^{(n)} \begin{cases} \max\limits_{\boldsymbol{s}} & \dfrac{|\alpha_r|^2 \left|\left(\boldsymbol{w}^{(n)}\right)^H (\boldsymbol{s} \odot \boldsymbol{p}_x)\right|^2}{\left(\boldsymbol{w}^{(n)}\right)^H \Sigma_{\boldsymbol{i}}(\boldsymbol{s}) \boldsymbol{w}^{(n)} + \sigma_n^2 ||\boldsymbol{w}^{(n)}||^2}. \\ s.t. & \boldsymbol{s} \in \Omega_M \end{cases} \tag{12}$$

Note that (11) is the well-known Minimum Variance Distortionless Response (MVDR) problem [33], and its solution can be obtained as

$$\boldsymbol{w}^{(n)} = (\Sigma_{\boldsymbol{i}}(\boldsymbol{s}^{(n)}) + \sigma_n^2 \boldsymbol{I})^{-1} (\boldsymbol{s}^{(n)} \odot \boldsymbol{p}_x). \tag{13}$$

Regarding to the Problem $\mathcal{P}_{\boldsymbol{s}}^{(n)}$, we consider the design of its entries consecutively, using the Coordinate Descent (CD) approach [34]–[37], which enables such an optimization by assuming one entry of the code vector $\boldsymbol{s} \in \mathbb{C}^N$ as the variable, keeping all the others fixed. By examining all the possible alphabet for the chosen variable, it selects the option which, with the correspondent filter, leads to the best SINR.

Mathematically, let s_d be the d^{th} code entry ($d = 1, ..., N$) and assume that it is the only variable, while the remaining $N-1$ entries are kept fixed and stacked into the $\boldsymbol{s}_{-d}$ vector as

$$\boldsymbol{s}_{-d} = [s_1, ..., s_{d-1}, s_{d+1}, ..., s_N]^T \in \mathbb{C}^{N-1}. \tag{14}$$

The design Problem $\mathcal{P}_{s_d}^{(k)}$, with respect to the variable s_d, can be expressed as

$$\mathcal{P}_{s_d}^{(n)} \begin{cases} \max\limits_{s_d} & f(s_d, \boldsymbol{s}_{-d}), \\ s.t. & s_d \in \Omega_M \end{cases} \tag{15}$$

which is still a non-convex, however, unlike the earlier formulation, it involves only one variable. Towards solving this, we calculate the SINR for each possible alphabet entry in Ω_M, and choose the one that results in the best value. In the next step, we perform this procedure for the next pulse s_{d+1}, and the process is repeated till all pulses are optimized at least once. The algorithm repeats the aforementioned steps until the stopping criteria is met. A good choice for that is when the SINR improvement, over one full optimization cycle of the code vector, is less then a pre-defined positive threshold, i.e. $(SINR^{(d)} - SINR^{(d-N)}) < \zeta$. Therefore, the optimized sequence $\boldsymbol{s}^\star$ can be obtained by

$$\boldsymbol{s}^{(k)} = [s_1^{(k)}, s_2^{(k)}, \ldots, s_N^{(k)}]^T. \tag{16}$$

Due to the iterative improvement, this framework guarantees that the SINR converges to the local optimum value [34], [38].

The general joint optimization procedure is described in Algorithm 1. It is important to notice that the calculation of the optimum filter coefficients $\boldsymbol{w}$ requires the specification of the target spatial Doppler vector $\boldsymbol{p}_x$ and the interference covariance matrix. Therefore, some previous knowledge about the desired signal is necessary, as well as the statistical characterization of the interfering signal. It is reasonable to assume that this knowledge can be provided from a previous Coherent Process Interval (CPI), with an uncoded (or possibly standard coded) transmission [19], and coarse estimation of the breathing and/or heartbeat frequencies. Then, our proposed joint optimization algorithm can be used for improving the SINR and, consequently, the estimation accuracy.

IV. Performance Analysis

In this Section we address the performance analysis of the proposed joint optimization algorithm by providing some numerical examples of its application. We consider a phase-coded 2.4 GHz radar system, with an uniform linear array of $N_a = 11$ elements, uniformly spaced ($d = \lambda/2$) and weighted. The number of interfering range and azimuth cells are assumed to be $N_c = 3$ and $L = 5$, respectively. The Signal to Noise Ratio (SNR) has been set up to be 10 dB,

Algorithm 1 Joint MPSK waveform and filter design, with CD approach

Input: $\boldsymbol{s}^{(0)}$, $\boldsymbol{p}_x$, $\sigma^2_{(r,k)}$, $\{\overline{\nu}_i,\epsilon\}$, σ_n^2 and $\zeta > 0$;
Output: Optimized waveform $\mathbf{s}^\star$ and correspondent filter $\boldsymbol{w}^*$;

1) **Initialization**.
   - Calculate $\boldsymbol{\Sigma}_i(\boldsymbol{s}^{(0)})$ from (7);
   - Calculate $\boldsymbol{w}(\boldsymbol{s}^{(0)})$ from (13);
   - Calculate $SINR^{(0)}$ from (6);
2) **Improvement**.
   - for each code entry d in $\boldsymbol{s}$:
     - for each alphabet entry i in Ψ_M:
       - Select s_i from Ψ_M, update $\Sigma_i(\boldsymbol{s})$, and calculate $\boldsymbol{w}_{(d,i)}$ and $SINR_{(d,i)}$;
     - Select $SINR_d^\star$ as the maximum of $SINR_{(d,i)}$;
     - $\boldsymbol{s}^{(d)} = \boldsymbol{s}_d^\star$;
     - $\boldsymbol{w}^{(d)} = \boldsymbol{w}_d^\star$;
     - $SINR^{(d)} = SINR_d^\star$;
3) **Stopping Criterion**.
   - If $(SINR^{(d)} - SINR^{(d-N)}) < \zeta$, stop. Otherwise go to the step 2;
4) **Output**.
   - Set $\boldsymbol{s}^\star = \boldsymbol{s}^{(d)}$ and $\boldsymbol{w}^\star = \boldsymbol{w}^{(d)}$.

while the Interference to Noise Ratio (INR) is 30 dB. The starting slow-time sequence is constant, which corresponds to the conventional design on the receiver side only. The stopping condition for the CD algorithm is set up to $\zeta = 10^{-3}$.

First, let us investigate the convergence behavior of the proposed algorithm, for different alphabet sizes. We consider a CPI of 5 seconds, with a Pulse Repetition Frequency (PRF) of 10 Hz. Therefore, the sequence size is $N = 50$. Fig. 2 shows the obtained SINR values versus the number of iterations, for a desired signal frequency of 12 bpm, which is a typical breathing rate. The interference mean Doppler is $\overline{\nu}_i = 0$, with uncertainty $\epsilon/2 = 10$ bpm, representing, for example, some random body motion in the vicinity of the chest-wall region. It can be seen that in each iteration, by performing the CD optimization procedure, the SINR increases monotonically and converges to a certain value. As expected, by increasing the alphabet size, the convergence behavior is improved. On the other hand, the variation of the final optimized SINR values is very small between the alphabets. This means that the optimization procedure is robust, even with very small alphabet sizes, including the binary case. Up to 4 dB of improvement could be obtained, even though this is an ideal case and, in a practical scenario, much smaller gains would be expected due to all the inaccuracies related to using the a priori information.

Fig. 3 shows the convergence behavior for different sequence sizes, and an alphabet size of $M = 4$. Due to the low frequency content of the breathing and heartbeat signals, large CPIs (usually 3 to 10 seconds) are required in order to acquire at least a few complete cycles of the desired signal

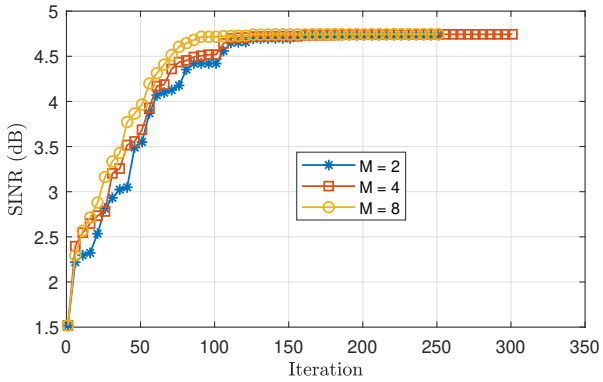

Fig. 2: Convergence behavior of the proposed optimization algorithm, for different MPSK alphabet sizes.

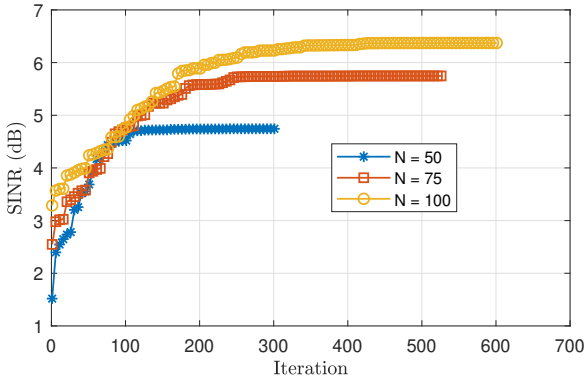

Fig. 3: Convergence behavior for the different sequence sizes, with $M = 4$.

and, therefore, long sequences are expected. It can be seen that the performance still improves up to 1.5 dB with the sequence increasing from $N = 50$ to $N = 100$, at the cost of an increasing convergence time as we will show soon.

The previous obtained SINR values are a composite result of the improvements from both the filter and sequence design. The behavior is also a function of the relative frequency between the desired signal and the interference. Those relations can be seen in the following analysis. Fig. 4 shows the SINR improvement exclusively due to the filter design using the MVDR approach, as a function of the desired signal frequency, for different variances of the interference Doppler. As an example, let us consider a frequency range from 0 bpm to 50 bpm, which fully covers the breathing region. The improvement is being calculated as the ratio of the SINR after and before the optimization procedure, i.e. the total improvement over all the iterations. It can be seen that when the desired signal and interference are well separated, the obtained improvement approaches the initial SINR, which means that the MVDR alone is able to totally suppress the interference. For theses cases, the waveform optimization makes little difference to the final result, as depicted in Fig.

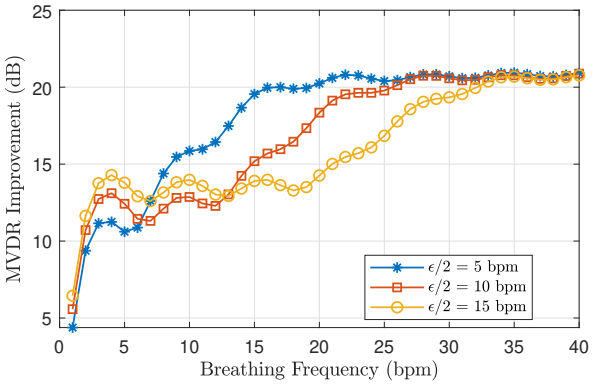

Fig. 4: MVDR improvement as a function of the desired signal frequency, for different interference variances.

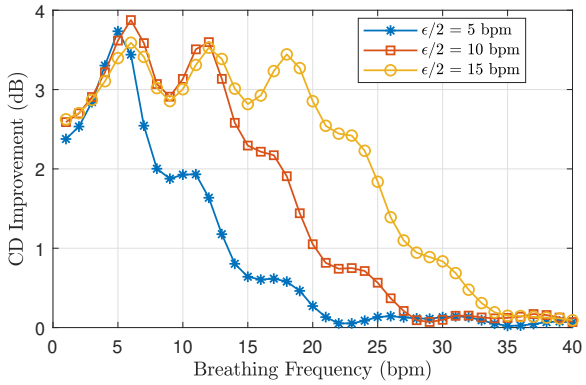

Fig. 5: Waveform design improvement as a function of the desired signal frequency, for different interference variances.

5, which shows the improvements only due to the slow-time waveform design. However, when the signal and interference are close to each other, a few extra dBs of improvement can be obtained by the sequence design, which then becomes an attractive solution.

Finally, Table I shows the convergence time for different alphabet sizes and sequence lengths, averaged over 10 independent trials. The reported values are obtained with a standard PC with Intel(R) Core(TM) i7-8650U CPU @ 1.90 GHz, with installed memory (RAM) 16.0 GB. Observe that within an specific sequence size, by increasing the alphabet size the convergence-time of proposed method increases. This behavior is expected, since the proposed method uses an entry by entry search strategy to find the optimum solution. It can also be seen that the convergence time also increases significantly with the sequence size as mentioned before.

TABLE I: Convergence Time (s)

M	N=50	N=75	N=100
2	0.47	1.89	4.36
4	1.12	3.37	8.47
8	1.63	6.51	15.83
16	3.91	10.98	32.59
32	8.06	27.48	65.61

V. Conclusion

This paper proposed a joint waveform and filter design for vital-sign estimation in phase-coded radar systems, with the objective of maximizing the SINR under signal-dependent interference. Through the modeling of the slow-time receiving signal, the design problem has been formulated as a multi-variable non-convex constrained optimization, and, as a solution to that, we used an MVDR filter with the Coordinate Descent approach to iteratively optimize the radar code, under the practical constraint of a discrete MPSK alphabet. The simulation results have shown monotonic increase of the SINR, with high suppression of the interference, and up to 4 dB of additional improvement with the sequence optimization, if compared to the conventional design on the receiver side only.

Acknowledgment

This work was supported by the National Research Fund of Luxembourg, under the AFR Industrial Fellowship Grant for Ph.D. projects (reference 14269859).

References

[1] M. Kebe, R. Gadhafi, B. Mohammad, M. Sanduleanu, H. Saleh, and M. Al-qutayri, "Human vital signs detection methods and potential using radars: A review," *Sensors (Switzerland)*, vol. 20, no. 5, 2020.

[2] C. Li, J. Cummings, J. Lam, E. Graves, and W. Wu, "Radar remote monitoring of vital signs," *IEEE Microwave Magazine*, vol. 10, no. 1, pp. 47–56, 2009.

[3] A. R. Diewald, J. Landwehr, D. Tatarinov, P. Di Mario Cola, C. Watgen, C. Mica, M. Lu-Dac, P. Larsen, O. Gomez, and T. Goniva, "RF-based child occupation detection in the vehicle interior," *Proceedings International Radar Symposium*, vol. 2016-June, pp. 1–4, 2016.

[4] S. Dias Da Cruz, H. P. Beise, U. Schroder, and U. Karahasanovic, "A Theoretical Investigation of the Detection of Vital Signs in Presence of Car Vibrations and RADAR-Based Passenger Classification," *IEEE Transactions on Vehicular Technology*, vol. 68, no. 4, pp. 3374–3385, 2019.

[5] J. K. Park, Y. Hong, H. Lee, C. Jang, G. H. Yun, H. J. Lee, and J. G. Yook, "Noncontact RF Vital Sign Sensor for Continuous Monitoring of Driver Status," *IEEE Transactions on Biomedical Circuits and Systems*, vol. 13, no. 3, pp. 493–502, 2019.

[6] J. Vicente, P. Laguna, A. Bartra, and R. Bailón, "Drowsiness detection using heart rate variability," *Medical and Biological Engineering and Computing*, vol. 54, no. 6, pp. 927–937, 2016.

[7] M. Alizadeh, H. Abedi, and G. Shaker, "Low-cost low-power in-vehicle occupant detection with mm-wave FMCW radar," *Proceedings of IEEE Sensors*, vol. 2019-Octob, no. 1, pp. 1–4, 2019.

[8] J. Yan, G. Zhang, H. Hong, H. Chu, C. Li, and X. Zhu, "Phase-Based Human Target 2-D Identification with a Mobile FMCW Radar Platform," *IEEE Transactions on Microwave Theory and Techniques*, vol. 67, no. 12, pp. 5348–5359, 2019.

[9] A. Al-Naji, K. Gibson, S. H. Lee, and J. Chahl, "Monitoring of Cardiorespiratory Signal: Principles of Remote Measurements and Review of Methods," *IEEE Access*, vol. 5, pp. 15 776–15 790, 2017.

[10] M. Nosrati and N. Tavassolian, "Accurate Doppler Radar-Based Cardiopulmonary Sensing Using Chest-Wall Acceleration," *IEEE Journal of Electromagnetics, RF and Microwaves in Medicine and Biology*, vol. 3, no. 1, pp. 41–47, 2019.

[11] C. Li and J. Lin, "Random body movement cancellation in doppler radar vital sign detection," *IEEE Transactions on Microwave Theory and Techniques*, vol. 56, no. 12, pp. 3143–3152, 2008.

[12] T. Sakamoto, R. Imasaka, H. Taki, T. Sato, M. Yoshioka, K. Inoue, T. Fukuda, and H. Sakai, "Feature-based correlation and topological similarity for interbeat interval estimation using ultrawideband radar," *IEEE Transactions on Biomedical Engineering*, vol. 63, no. 4, pp. 747–757, 2016.

[13] M. Nosrati and N. Tavassolian, "High-Accuracy Heart Rate Variability Monitoring Using Doppler Radar Based on Gaussian Pulse Train Modeling and FTPR Algorithm," *IEEE Transactions on Microwave Theory and Techniques*, vol. 66, no. 1, pp. 556–567, 2018.

[14] J. J. Saluja, J. J. Casanova, and J. Lin, "A Supervised Machine Learning Algorithm for Heart-rate Detection Using Doppler Motion-Sensing Radar," *IEEE Journal of Electromagnetics, RF and Microwaves in Medicine and Biology*, vol. 4, no. 1, pp. 45–51, 2019.

[15] V. L. Petrovic, M. M. Jankovic, A. V. Lupsic, V. R. Mihajlovic, and J. S. Popovic-Bozovic, "High-Accuracy Real-Time Monitoring of Heart Rate Variability Using 24 GHz Continuous-Wave Doppler Radar," *IEEE Access*, vol. 7, pp. 74 721–74 733, 2019.

[16] K. V. Mishra, M. R. Bhavani Shankar, V. Koivunen, B. Ottersten, and S. A. Vorobyov, "Toward Millimeter-Wave Joint Radar Communications: A signal processing perspective," *IEEE Signal Processing Magazine*, vol. 36, no. 5, pp. 100–114, 2019.

[17] S. Saponara, M. S. Greco, and F. Gini, "Radar-on-Chip/in-Package in Autonomous Driving Vehicles and Intelligent Transport Systems: Opportunities and Challenges," *IEEE Signal Processing Magazine*, vol. 36, no. 5, pp. 71–84, 2019.

[18] S. Z. Gurbuz, H. D. Griffiths, A. Charlish, M. Rangaswamy, M. S. Greco, and K. Bell, "An Overview of Cognitive Radar: Past, Present, and Future," *IEEE Aerospace and Electronic Systems Magazine*, vol. 34, no. 12, pp. 6–18, 2019.

[19] A. Aubry, A. De Maio, A. Farina, and M. Wicks, "Knowledge-aided transmit signal and receive filter design in signal-dependent clutter," *Waveform Design and Diversity for Advanced Radar Systems*, vol. 49, no. 1, pp. 497–534, 2012.

[20] E. Raei, M. Alaee-kerahroodi, B. S. M. R, and B. Ottersten, "Designing MPSK Sequences and Doppler Filter Bank in Cognitive Radar Systems," *2019 IEEE Radar Conference, RadarConf 2019*, no. 1, 2019.

[21] M. Alaee-Kerahroodi, M. Modarres-Hashemi, and M. M. Naghsh, "Designing Sets of Binary Sequences for MIMO Radar Systems," *IEEE Transactions on Signal Processing*, vol. 67, no. 13, pp. 3347–3360, 2019.

[22] M. A. Richards, *Fundamentals of radar signal processing*. Tata McGraw-Hill Education, 2014.

[23] A. Ahmad, J. C. Roh, D. Wang, and A. Dubey, "Vital signs monitoring of multiple people using a FMCW millimeter-wave sensor," *2018 IEEE Radar Conference, RadarConf 2018*, no. 4, pp. 1450–1455, 2018.

[24] C. Li, V. M. Lubecke, O. Boric-Lubecke, and J. Lin, "A review on recent advances in doppler radar sensors for noncontact healthcare monitoring," *IEEE Transactions on Microwave Theory and Techniques*, vol. 61, no. 5, pp. 2046–2060, 2013.

[25] J. Tu and J. Lin, "Fast acquisition of heart rate in noncontact vital sign radar measurement using time-window-variation technique," *IEEE Transactions on Instrumentation and Measurement*, vol. 65, no. 1, pp. 112–122, 2016.

[26] L. Sun, S. Huang, Y. Li, C. Gu, H. Pan, H. Hong, and X. Zhu, "Remote Measurement of Human Vital Signs Based on Joint-Range Adaptive EEMD," *IEEE Access*, vol. 8, pp. 68 514–68 524, 2020.

[27] A. De Groote, M. Wantier, G. Cheron, M. Estenne, and M. Paiva, "Chest wall motion during tidal breathing," *Journal of Applied Physiology*, vol. 83, no. 5, pp. 1531–1537, 1997.

[28] J. Kranjec, S. Beguš, G. Geršak, and J. Drnovšek, "Non-contact heart rate and heart rate variability measurements: A review," *Biomedical Signal Processing and Control*, vol. 13, no. 1, pp. 102–112, 2014.

[29] A. Aubry, A. De Maio, and M. M. Naghsh, "Optimizing Radar Waveform and Doppler Filter Bank via Generalized Fractional Programming," *IEEE Journal on Selected Topics in Signal Processing*, vol. 9, no. 8, pp. 1387–1399, 2015.

[30] L. Zhao and D. P. Palomar, "Maximin Joint Optimization of Transmitting Code and Receiving Filter in Radar and Communications," *IEEE Transactions on Signal Processing*, vol. 65, no. 4, pp. 850–863, 2017.

[31] C. Li and J. Lin, "Complex signal demodulation and random body movement cancellation techniques for non-contact vital sign detection," *IEEE MTT-S International Microwave Symposium Digest*, pp. 567–570, 2008.

[32] M. Alaee-Kerahroodi, S. Imani, M. R. Bhavani Shankar, M. M. Nayebi, and B. Ottersten, "A coordinate descent framework to joint design of MPSK sequences and receive filter weights in MIMO radar systems," *2019 IEEE Radar Conference, RadarConf 2019*, 2019.

[33] J. Capon, "High-Resolution Frequency-Wavenumber Spectrum Analysis," vol. 57, no. 8, pp. 1408–1418, 1969.

[34] S. J. Wright, "Coordinate descent algorithms," *Mathematical Programming*, vol. 151, no. 1, pp. 3–34, 2015.

[35] M. Alaee-Kerahroodi, A. Aubry, A. De Maio, M. M. Naghsh, and M. Modarres-Hashemi, "A coordinate-descent framework to design low PSL/ISL sequences," *IEEE Transactions on Signal Processing*, vol. 65, no. 22, pp. 5942–5956, 2017.

[36] M. Alaee-Kerahroodi, M. Modarres-Hashemi, and M. M. Naghsh, "Designing sets of binary sequences for MIMO radar systems," *IEEE Transactions on Signal Processing*, vol. 67, no. 13, pp. 3347–3360, 2019.

[37] M. M. Feraidooni, D. Gharavian, M. Alaee-Kerahroodi, and S. Imani, "A coordinate descent framework for probing signal design in cognitive mimo radars," *IEEE Communications Letters*, pp. 1–1, 2020.

[38] B. Chen, S. He, Z. Li, and S. Zhang, "Maximum block improvement and polynomial optimization," *SIAM Journal on Optimization*, vol. 22, no. 1, pp. 87–107, Jan 2012.